

# Lidar system upgrade at Atmospheric Rome joint supersite (ARTE)

Giuliano, G.<sup>(a)</sup>, Dionisi, D.<sup>(a)</sup>, Di Paolantonio, M.<sup>(a,b)</sup>, Liberti, G. L.<sup>(a)</sup>

<sup>(a)</sup> Institute of Marine Sciences, Italian National Research Council (ISMAR-CNR), 00133 Rome, Italy

<sup>(b)</sup> School of Engineering, University of Basilicata, 85100 Potenza, Italy

Lead Author e-mail address: [giovanni.giuliano@cnr.it](mailto:giovanni.giuliano@cnr.it)

**Abstract:** The Rome Tor Vergata Lidar Rayleigh-Mie-Raman (RMR), multi-channel/multi-telescope, transportable and with a modifiable configuration, was built in 1999. Since 2002 it has been operating in the Consiglio Nazionale delle Ricerche (CNR) research area in Rome Tor Vergata in the following main research areas: upper atmosphere physics, interactions between water vapor-aerosol-clouds and study of planetary boundary layer processes. This work describes the extraordinary maintenance and upgrading activities to adapt the system to the advanced technological solutions and to the operating mode to meet the requirements within the framework of the labelling process as a Centre for Aerosol Remote Sensing - Aerosol, Clouds and Trace Gases Research Infrastructure (CARS-ACTRIS) National Facilities.

## 1. Introduction

In the context of networks of high performance lidar-based national facilities (NFs) (e.g. ACTRIS/EARLINET, the Aerosol, Clouds and Trace Gases Research Infrastructure/European Aerosol Research Lidar Network), there is a need to define standard quality assurance procedures for NF operation. The multi-wavelength multi-telescope Rayleigh-Mie-Raman (RMR) system at the CNR research area of Rome - Tor Vergata was designed and developed in the mid-90s [1] with a focus on geophysical variables in the mid/upper atmosphere [2-4]. This system is now included as a NF of the Atmospheric Rome joint supersite (ARTE) for the Aerosol Remote Sensing (ARS) component. Therefore, an overview of the advanced technological solutions implemented for such high-power lidar system is presented here.

## 2. System description

The system, shown in Figure 1, is assembled in two stacked containers. The emitter component consists of a Nd:YAG laser source that, currently, emits two beams at 355 and 532 nm that are collimated by means of 5x beam expanders and are projected vertically into the atmosphere by two 45° mirrors that can be Azimuth and Zenith oriented through computer-controlled stepping motors. The receiver is based on a multiple-telescope configuration, which allows the sounding of a

wide altitude atmospheric interval. A system of three orthogonal linear-stages allows each box to be moved along the X, Y and Z axes by computer-controlled stepping motors to find the optimum alignment and focusing positions autonomously for each telescope. There are a total of 37 servomotors (three for each telescope and two for each emitted wavelength) are present.

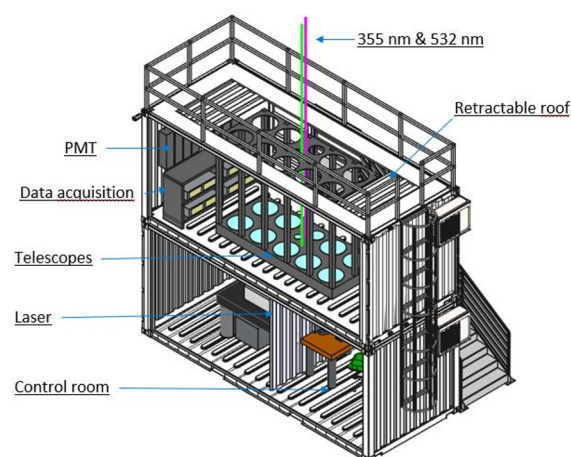


Figure 1. Overview of the high-power lidar installed at ARTE.

As summarized in Table 1, the use of 11 separate Newtonian f/3 telescopes (two single with diameters of 150 mm and 300 mm, and an array of nine 500 mm telescopes) mounted at different positions relative to the emitters, provides the possibility of targeting different altitude ranges of interest depending on the geophysical variables [5]. The full overlap values for the telescope array are given for the

telescopes closer and further to the emitted beams. Using a telescope with a small aperture (150 mm) and a full angle field of view (FOV) of 1.8 mrad, it is possible to achieve a full overlap height of less than 300 m.

**Table 1. Telescope characteristics**

Telescope	#1	#2	#3
Type	Array of nine	Single	Single
Diameter (mm)	500 (each)	300	150
Focal length (mm)	1500	900	450
FOV (mrad)	0.5	0.9	1.8
Full overlap (m)	From 4000 to 8000	< 1000	< 300

A semi-automated mapping procedure [6] was developed to control both the signal acquisition and the 3D motor movements (*i.e.* diaphragm position) around the focal point of the telescopes in order to optimize the telescope/beam alignment and thus increase the signal, to estimate the overlap function  $O(R)$  and to better characterize the dependence of the acquired signal on the relative transmitter-receiver geometry of the system.

System upgrades included state-of-the-art components, as well as the installation of a new high-energy Nd:YAG laser (Continuum Powerlite DLS 8010, pulse repetition rate 10 Hz) with second (532 nm) and third (355 nm) harmonic generators. The energy output is optimized for the investigation of the UV Raman scattering, with pulse energies of approximately 450 mJ and 240 mJ, respectively.

Up to late 2022, the 150 mm telescope detected only the total elastic backscattering signal at 532 nm. The 300 mm telescope had UV channels Raman molecular nitrogen and water vapor (WV) low range and the elastic channel at 355 nm plus the elastic midrange 532 nm. The 150 mm and 300 mm telescopes operate in daytime and night-time configuration while the

use of the 9 telescope array is limited to nighttime. The former configuration is used for EARLINET standard measurement sessions. In order to meet the technical specifications of ACTRIS, the 150 mm and 300 mm telescope channels have recently undergone specific upgrades and tests based on the characteristics of the system.

### 3. Receiving optical system

A major design change in the system upgrade was the replacement of the small optical system boxes located at the focus of the 150 mm and 300 mm telescopes. New multi-wavelength separation units, shown in Figure 2, and polarization calibrator are mounted above two telescopes with a remotely operated electric shutter to perform dark measurements for each telescope [7].

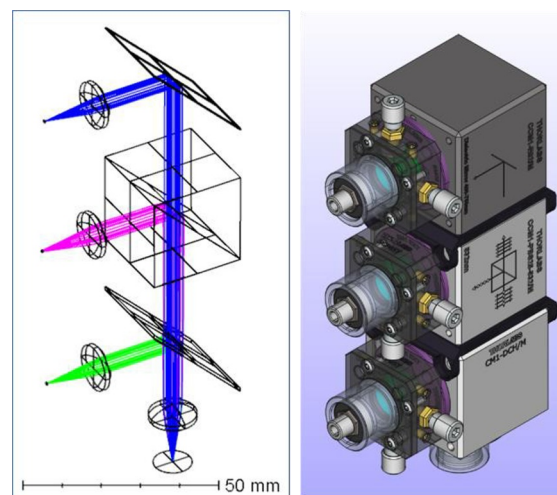


Figure 2. (left) Ray-tracing simulations and (right) CAD of the multi-wavelength separation unit.

Due to the additional length of the new optical boxes, a mechanical modification of the two columns supporting the telescopes was required: currently the telescopes are mounted on height-adjustable columns to allow different configurations. The returning lidar beam, after the field stop diaphragm (fixed 0.8 mm for the 150 mm telescope and 0.2, 0.4, 0.6, 0.8 mm diameter for the 300 mm telescope), is first collimated by a plano-convex lens and then separated into its UV, visible and IR wavelength components by an appropriate combination of optics (harmonic beamsplitter, polarizing dichroic beamsplitter cube and turning mirror) specifically designed to separate the harmonics of Nd:YAG laser sources and

with antireflection coatings to minimize the optical losses throughout the optical path.

As shown in Figure 2 (left), a plano-convex lens is placed in front of each optical fibre (0.94 mm core diameter and 0.22 numerical aperture) to focus the separated wavelengths onto the input face of each fibre. Neutral density (ND) filters are placed at the photomultiplier tube (PMT) window to prevent blinding from the strong return from low altitudes. Each multi-wavelength separation unit was aligned on an optical bench before being mounted on the lidar system. The upgraded design of the optical system for the 150 and 300 mm telescopes allows the number of detection channels to be increased five to twelve (summarized in Table 2) to meet the requirements of  $1\beta + 1\alpha + 1\delta$  at 355 nm.

**Table 2. Upgraded channels details**

New CH ID	Telescope Diameter (mm)	$\lambda$ (nm)	Type
1, 7	150, 300	354.7	Elastic transmitted
2, 8		354.7	Elastic reflected
3, 9		386.7	N <sub>2</sub> Raman
4, 10		407.5	H <sub>2</sub> O Raman
5, 11		532.1	Elastic
6, 12		607.6	N <sub>2</sub> Raman

The light exiting from the optical fibers is collimated and, after passing through the appropriate narrow-band interference filter, is directed to the photomultiplier (PMT). A schematic of a new fiber-optic three-wavelength separation assembly is shown in Figure 3.

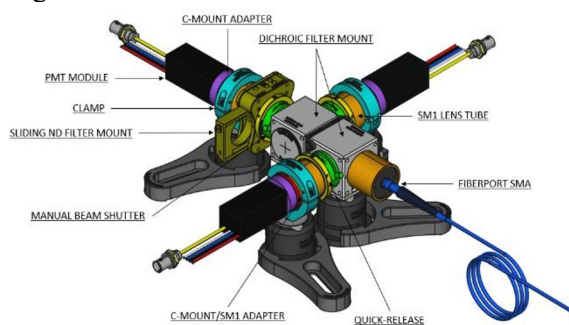


Figure 3. Schematic of the optical separation assembly for a 3-channel sub-system.

All twelve channels listed in Table 2 are equipped with brand new state-of-the art Hamamatsu optical sensor modules containing a metal package PMT and a high-voltage power supply circuit. The model of each channel has been selected according to the maximum responsivity at the wavelength of interest and all PMTs have been selected with the low dark count variation, which is specific for photon counting measurements.

In order to drive and control up to 16 PMTs, a low-voltage power supply unit has been designed and developed with EMI shielding and data logging of the control voltage (*i.e.* PMT gain) applied to each module throughout the measurement session.

#### 4. System remote control

As shown in Figure 1, the control room is located on the right side of the lower container. Data from the various devices in the lidar system is transmitted to the main control unit, which is equipped with custom LabVIEW software and all the necessary drivers to communicate and control the I/O devices connected to the PC.

The development of custom LabVIEW software for remote power-up and power-down, remote instrument control, measurement scheduling, data acquisition and real-time data visualization allows to have a high degree of remote control on the main components of the lidar. The operation of the sliding roof is managed by an Ethernet relay controlling the two worm gear motors, one for each side of the roof, and the whole operation can be monitored via a webcam.

#### 5. Acknowledgments

This project was supported by IR0000032 – ITINERIS, Italian Integrated Environmental Research Infrastructures System (D.D. n. 130/2022 - CUP B53C22002150006) Funded by EU - Next Generation EU PNRR- Mission 4 “Education and Research” - Component 2: “From research to business” - Investment 3.1: “Fund for the realisation of an integrated system of research and innovation infrastructures”.

## 6. References

- [1] Congeduti, F., Marengo, F., Baldetti, P., Vincenti, E., "The multiple-mirror lidar '9-eyes'", *J. Opt. A: Pure Appl. Opt.* 1, 185 (1999).
- [2] Dionisi, D., and Coatuors, "Calibration of a multichannel water vapor Raman lidar through noncollocated operational soundings: optimization and characterization of accuracy and variability", *JTECH* 27.1, 108-121 (2010).
- [3] Dionisi, D., Keckhut, P., Hoareau, C., Montoux, N., Congeduti, F., "Cirrus crystal fall velocity estimates using the Match method with ground-based lidars: first investigation through a case study", *AMT*, 6, 457–470 (2013).
- [4] Dionisi, D., Keckhut, P., Liberti, G. L., Cardillo, F., Congeduti, F., "Midlatitude cirrus classification at Rome Tor Vergata through a multichannel Raman–Mic–Rayleigh lidar", *ACP*, 13, 11853–11868 (2013).
- [5] Liberti, G. L., Dionisi, D., Cheruy, F., Risi, C., "Feasibility study to measure HDO/H<sub>2</sub>O atmospheric profiles through a Raman lidar", *ILRC28 EPJ Web of Conferences*, 176 , 05032. 4 pp. (2018).
- [6] Di Paolantonio, M., Dionisi, D., Liberti, G. L., "A semi-automated procedure for the emitter-receiver geometry characterization of motor-controlled lidars", *AMT*, 15, 1217-1231 (2022).
- [7] Freudenthaler, V., "About the effects of polarising optics on lidar signals and the  $\Delta 90$  calibration", *AMT*, 9, 4181-4255 (2016).